科学通报 2017 年 第 62 卷 第 4 期: 298 ~ 311
论 文
《中国科学》杂志社
SCIENCE CHINA PRESS

藏南床得剖面古地磁结果对印度-亚洲碰撞方式的约束

张波兴, 李永祥*, 胡修棉

南京大学地球科学与工程学院, 内生金属矿床成矿机制研究国家重点实验室, 南京 210023
* 联系人, E-mail: yxli@nju.edu.cn

2016-09-01 收稿, 2016-10-12 修回, 2016-10-13 接受, 2017-01-03 网络版发表
国家自然科学基金(41274071, 41525007)和国家重点基础研究发展计划(2012CB822001)资助

摘要 特提斯喜马拉雅位于大印度最北端, 其构造演化是理解印度-亚洲大陆碰撞过程的关键之一. 为了更好地限定特提斯喜马拉雅中生代以来的古地理位置及其漂移历史, 本文对藏南江孜床得剖面侏罗系下热组、维美组和白垩系床得组开展了古地磁研究. 古地磁样品取自39个采样点, 其中下热组5个, 岩性为青灰色安山岩; 维美组25个, 岩性为粉砂岩和砂岩; 床得组9个, 岩性为灰岩. 对118个古地磁柱状样品进行的逐步热退磁和交变退磁结果显示, 下热组和维美组样品未能分离出稳定的特征剩磁; 床得组样品分离出了稳定的特征剩磁(ChRM), 且具有正反极性, 并通过了倒转检验. 结合沉积学和岩石磁学结果, 床得组样品的特征剩磁很可能为原生剩磁, 其年龄为86.3~74.0 Ma. 床得组样品特征剩磁的平均方向为D_s=152.0°, I_s=–52.9°, κ=18.0, α_{95}=5.9°. 该数据表明, 特提斯喜马拉雅江孜地区在晚白垩世(80.1±6.2 Ma)所处的古纬度为南纬33.1°±5.6°, 与印度板块北缘同时代所处的古纬度一致(参考点28.0°N, 88.5°E), 说明二者至少在晚白垩世之前从运动学意义上仍然是一个块体, 缺乏大洋分隔的证据. 这为理解印度-亚洲大陆碰撞方式提供了新的古地磁约束.

关键词 藏南, 床得剖面, 特提斯喜马拉雅, 晚白垩世, 古地理, 古地磁

在过去几十年间, 围绕印度-亚洲大陆碰撞发生的时间[1~11]、碰撞发生的古地理位置[2,7~9,12~15]、碰撞的方式[7,12,16~21]等科学问题, 前人开展了大量研究工作, 在认识这一重大地质事件的发展演化过程方面取得了长足进展. 同时, 深入的研究工作也表明, 碰撞过程可能比以往认识的更复杂. 就碰撞方式而言, 传统模式认为, 雅鲁藏布缝合带是大印度板块与亚洲大陆碰撞导致新特提斯洋关闭的接合带[22~24], 其北侧的拉萨地块在两大陆碰撞前是亚洲大陆的南缘, 其南侧的特提斯喜马拉雅是大印度板块的北缘[23](图1(a)). 在传统模式中, 特提斯喜马拉雅在印度-亚洲大陆碰撞之前一直作为印度板块的一部分, 并没有发生过分离[6,12]. 而近年来, 有学者提出, 位于大印度板块最北端的特提斯喜马拉雅与大印度板块主体(印度板块)先发生分离并与拉萨地块在大约50 Ma发生第一次碰撞, 然后印度板块与特提斯喜马拉雅在~23 Ma时发生第二次碰撞[7], 即所谓的“双碰撞”模式. 最近, Yang等人[20]和Ma等人[21]从特提斯喜马拉雅获得了高质量的早白垩世(~130 Ma)古地磁数据, 认为特提斯喜马拉雅与印度板块在早白垩世时是一个整体, 在晚白垩世时发生了分离, 之后发生了两次碰撞, 并认为支持“双碰撞”模式. 然而, 对于该模式的关键环节, 即二者在晚白垩世时发生分离, 目前仍然只是推测, 并没有充分的地质和古地磁方面的约束. 因此, “双碰撞”模式尚需进一步检验. 显然, “双碰撞”模式与传统模式的最大分歧在于特提斯喜马拉雅是否与印度板块发生过分离以及何时分离.

古地磁研究是重建板块古地理位置的重要方法,

引用格式: 张波兴, 李永祥, 胡修棉. 藏南床得剖面古地磁结果对印度-亚洲碰撞方式的约束. 科学通报, 2017, 62: 298–311
Zhang B X, Li Y X, Hu X M. Paleomagnetic results from Jurassic-Cretaceous strata in the Chuangde area of southern Tibet constrain the nature and timing of the India-Asia collision system (in Chinese). Chin Sci Bull, 2017, 62: 298–311, doi: 10.1360/N972016-00767

可以用来重建特提斯喜马拉雅的构造演化过程，进而检验它是否与印度板块发生了分离等. 事实上，古地磁方法已应用到确定特提斯喜马拉雅的古纬度、运动学特征等方面[1,6,12,20,21,25,28]. 虽然前人已经对特提斯喜马拉雅侏罗纪-古新世的岩石地层做了很多古地磁研究[6,12,25,28~30]，但由于广泛存在的重磁化[28,31]，可靠的原生剩磁结果较少. 此外，目前用于约束特提斯喜马拉雅的古地磁数据大都来自早白垩世和古近纪[6,20,21,25,30]，缺乏可靠的侏罗纪末期和晚白垩世古地磁数据，导致对特提斯喜马拉雅与印度板块是否发生过分离、分离的具体时间等科学问题仍不能准确厘定. 因此，获得可靠的侏罗纪末期和晚白垩世的古地磁数据就显得尤为重要.

本文对藏南江孜地区床得剖面侏罗-白垩系地层开展了古地磁研究，旨在获得特提斯喜马拉雅侏罗-晚白垩世可靠的古地磁数据，进一步约束其古地理位置及漂移历史，并探讨其与印度板块之间的关系. 同时，新的古地磁结果也将为探讨印度板块与亚洲大陆的碰撞方式提供新约束.

1 地质背景和样品采集

特提斯喜马拉雅位于藏南拆离系(STDS)和印度-雅鲁藏布江缝合带(ITSZ)之间，是一东西长约2000 km而南北狭窄的地质构造单元(图1(a)). 以吉隆-康马断层为界可将该构造单元分为南带和北带两部分. 南带主要是浅水陆架碳酸盐和陆相沉积的古生界到始新统地层[32,33]，北带则主要出露有中生代到古新世的深水外陆架、大陆斜坡和陆隆沉积[26,32]. 同时，古生代-中生代的火山岩在特提斯喜马拉雅也有广泛出露[34,35]. 本文研究剖面位于藏南江孜县城至仁布县公路旁的床得村(28.9°N，89.7°E，海拔4292 m)(图1(b))，距离江孜县城东北约15 km，沉积地层特征属特提斯喜马拉雅的北带[26].

前人已对该剖面进行过野外地质调查、剖面实测、化石鉴定、沉积岩石学分析等地层学和年代学以及沉积环境演化等方面的工作[27,36~38]，为深入的古地磁工作奠定了基础. 床得剖面出露中侏罗统——上白垩统地层(图1(c))，为江孜背斜的南翼，地层倾向逐渐由北西转为南东. 剖面最下部为下热组(未见底)，主要由青灰色安山岩、安山玄武岩组成，厚度约50 m，其时代应属中侏罗世[27]. 下热组安山岩地层产状是用上覆维美组地层的产状来确定的. 覆于其上的维美组，地层发生倒转，倾向向北，总厚度约170 m. 其下部为褐黄、灰黑色硅质岩与泥灰岩；上部由黄绿、灰黑色页岩与灰白色砂岩组成. 维美组之上为甲不拉组，根据风化色的不同可分为黑层段和白层段. 黑层段层序倒转，以黑色页岩为主，厚度约为55 m，生物组合特征显示其为下白垩统地层[37]；白层段层序正常，倾向向南，岩性以页岩为主夹硅质、钙质页岩，厚约60 m，化石带特征显示其时代相当于晚白垩世赛诺曼期(Cenomanian)至土伦期(Turonian)[37]. 床得组由砖红色、紫红色、褐红色叶片状页岩、泥岩、中-厚层泥灰岩和粉砂质、砂质灰岩组成，厚度约30 m，位于甲不拉组之上，层序正常，是沉积于富氧环境下形成的白垩纪大洋红层[39]. 沉积构造及微体古生物分析床得组中的泥质灰岩为浊流沉积，灰岩沉积环境为斜坡相，且发生了滑塌[39]. 根据对床得组浮游有孔虫分析，其时代为白垩纪晚三冬期(late Santonian)至中坎潘期(middle Campanian)[40]. 床得剖面最上部的宗卓组，为混杂堆积，厚度超过150 m.

由于甲不拉组为泥页岩等，风化破碎严重，无法取样. 我们分别从下热组、维美组和床得组采集了古地磁样品. 一共布设了39个采点，其中下热组5个采样点(XR1~XR5)共11块手标本，均为青灰色安山岩；维美组25个采样点(WM1~WM25)共61块手标本，主要采自粉砂岩层和砂岩层，少数几个为硅质页岩；床得组9个采样点(CHD1~CHD9)共40块手标本，岩性主要为灰岩. 因下热组和维美组地层发生倒转，受构造影响较大，且岩性较为破碎，手标本采集较少. 手标本用罗盘定向. 研究区的磁偏角为0.13°[41]，可以忽略不计. 在实验室将手标本画好定向标志线之后，用台式钻机以垂直于手标本表面的方法钻取圆柱样，并用切割机加工出118个标准的古地磁圆柱样品(直径2.5 cm，高2.2 cm).

2 实验方法

在实验室，首先用KLY-3S卡帕桥测量样品的磁化率各向异性(AMS). 之后分别用ASC-TD 48型热退磁炉(炉内磁场强度小于10 nT)和Molspin交变退磁仪对样品进行逐步热退磁和交变退磁. 逐步热退磁实验在低温段(<300℃)温度间隔设置为50℃，为了更加精确地获得特征剩磁方向，在高温段将温度间隔设为20℃或30℃，最终逐步加热至540~580℃或680℃，

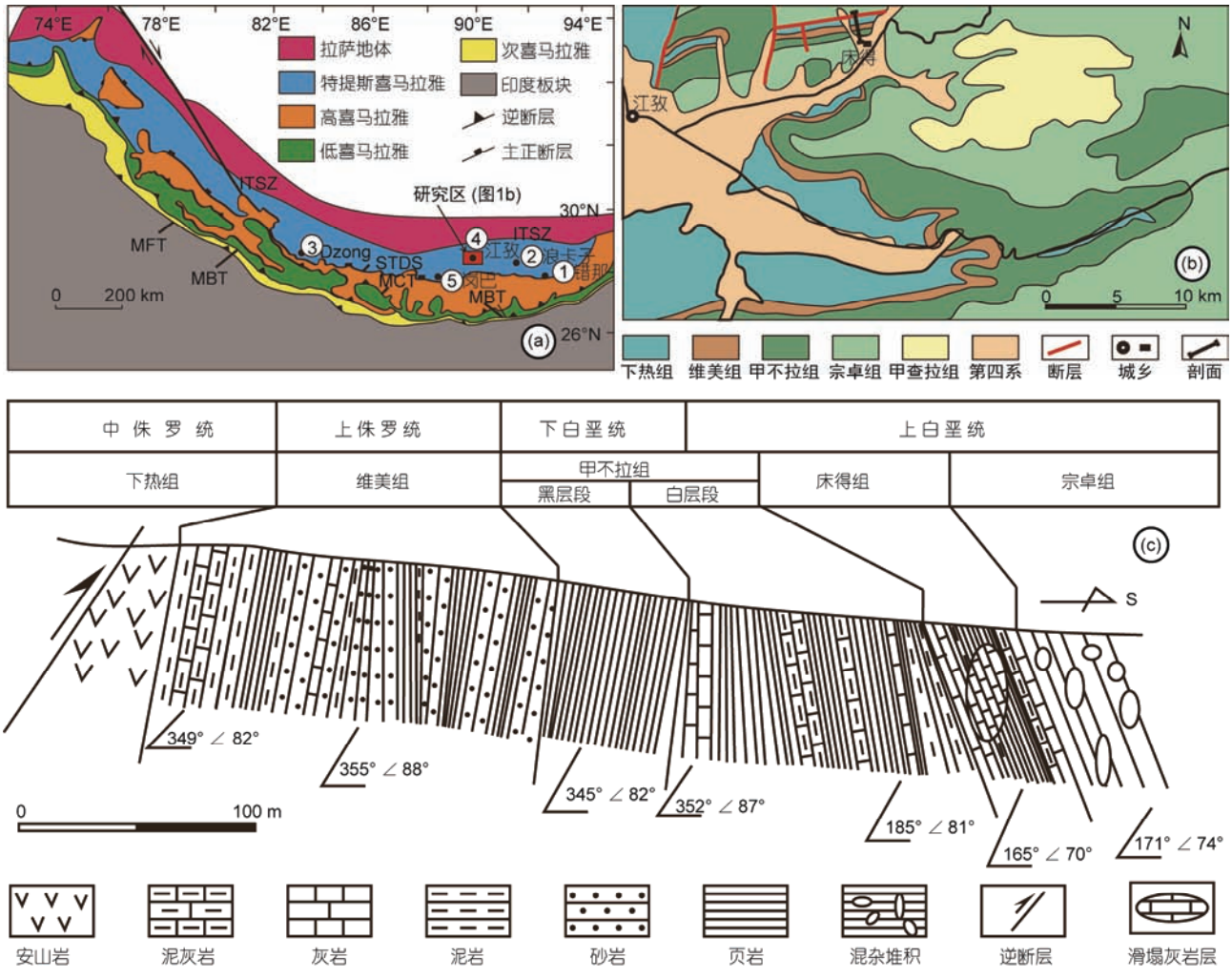

图 1 特提斯喜马拉雅、床得剖面及其周边区域地质图((a), (b))和床得剖面简图(c). (a) 据Hu等人[11]修改; ITSZ, 印度-雅鲁藏布江缝合带; STDS, 藏南拆离系; MCT, 主中央逆断层; MBT, 主边界逆断层; MFT, 主前缘逆断层; 实心圆点表示前人及本文获得古地磁数据的采样地区: ①, 错那(Yang等人[20]); ②, 浪卡子(Ma等人[21]); ③, Dzong (Klootwijk等人[25]); ④, 江孜(本文); ⑤, 岗巴(Yi等人[6], Patzelt等人[12]). (b) 据Hu等人[26]; (c) 据李祥辉等人[27]修改

Figure 1 Simplified geologic maps of the study area. (a) Regional geologic map of southern Tibet showing major tectonic units including Tethyan Himalaya (in blue) in which the studied Chuangde section is situated (after Hu et al.[11]). (b) Geologic map showing the Mesozoic strata of the study area and the location of the Chuangde section (after Hu et al.[26]). (c) The cross-section of Chuangde section (after Li et al.[27]). ITSZ, Indus-Tsangpo suture zone; STDS, South Tibet detachment system; MCT, Main Central thrust; MBT, Main Central thrust; MFT, Main Frontal thrust. The solid points mark the sampling locations of Paleomagnetic studies. ① Cuona (Yang et al.[20]), ② Langkazi (Ma et al.[21]), ③ Dzong (Klootwijk et al.[25]), ④ Jiangzi (this study), ⑤ Gamba (Yi et al.[6], Patzelt et al.[12])

直至天然剩磁强度低于初始强度的5%. 交变退磁实验在20 mT以前间隔为5 mT, 20 mT以后间隔改为10 mT直至90~100 mT. 剩磁的测试使用美国2G公司生产的2G-755超导磁力仪. 退磁结果用正交投影图展示[42], 并用主成分分析法对不同磁成分进行拟合、分离[43], 剩磁的平均方向使用Fisher统计法进行统计[44]. 在分析古地磁数据过程中使用了PMGSC[45]和PaleoMac[46]等软件.

另外, 为了研究样品中的载磁矿物, 对床得组代表性样品进行了一系列岩石磁学分析. 磁化率-温度曲线利用KLY-3S卡帕桥和与其配套的CS-3加热装置测得. 等温剩磁(IRM)获得曲线由ASC IM-10-30型脉冲磁力仪(最大磁场强度2.4 T)和JR-6A型旋转磁力仪结合使用测得; 三轴等温剩磁热退磁实验使用ASC IM-10-30型脉冲磁力仪分别给样品的*Z*轴、*Y*轴和*X*轴施加2.4, 0.4和0.12 T的磁场, 然后逐步热退磁并利用

JR-6A型旋转磁力仪进行测试. 所有古地磁和岩石磁学实验均在南京大学古地磁实验室完成(磁屏蔽屋内磁场强度小于300 nT).

3 实验结果

3.1 磁化率各向异性(AMS)

在地层坐标系下, 下热组样品AMS结果显示磁化率椭球体的最大轴近似于垂直层面, 而中间轴和最小轴与层面平行(图2(a)). 维美组样品的磁化率椭球体的3个主轴随机散乱分布(图2(b)), 无法判断其磁组构类型. 床得组样品磁化率椭球体最小轴近似垂直于层面, 而最大轴和中间轴则较为集中地近似于水平分布在层面上, 其中最大轴方位集中在东南方向, 中间轴的主要方向则为北偏东(图2(c)). Flinn图显示大部分样品为扁平组构, 少部分样品为弱棒状组构(图2(d)), 可能指示受水流影响. 综合来看, 床得组结果显示为沉积类型磁组构.

3.2 岩石磁学结果

床得组典型样品的磁化率-温度变化曲线显示, 降温过程的磁化率高于升温过程的磁化率, 说明加热过程中出现了矿物相转化[47]. 加热曲线特征有两类. 一类是磁化率在550℃之前逐渐下降, 在580~600℃时出现陡降, 达到最低值(图3(a), (c)), 表明样品中有磁铁矿; 另一类是磁化率在580℃之前逐渐下降, 580℃之后下降较快, 600~700℃逐渐下降, 并在700℃时降至最低点, 表明样品中可能含有赤铁矿和磁铁矿(图3(b), (d)). 等温剩磁获得曲线显示样品分为两类. 一类是在~500 mT时, 其剩磁强度接近饱和; 另一类样品随着外加磁场的增加直到2.4 T剩磁强度仍然没有饱和(图4(a)). 等温剩磁获得曲线结果表明

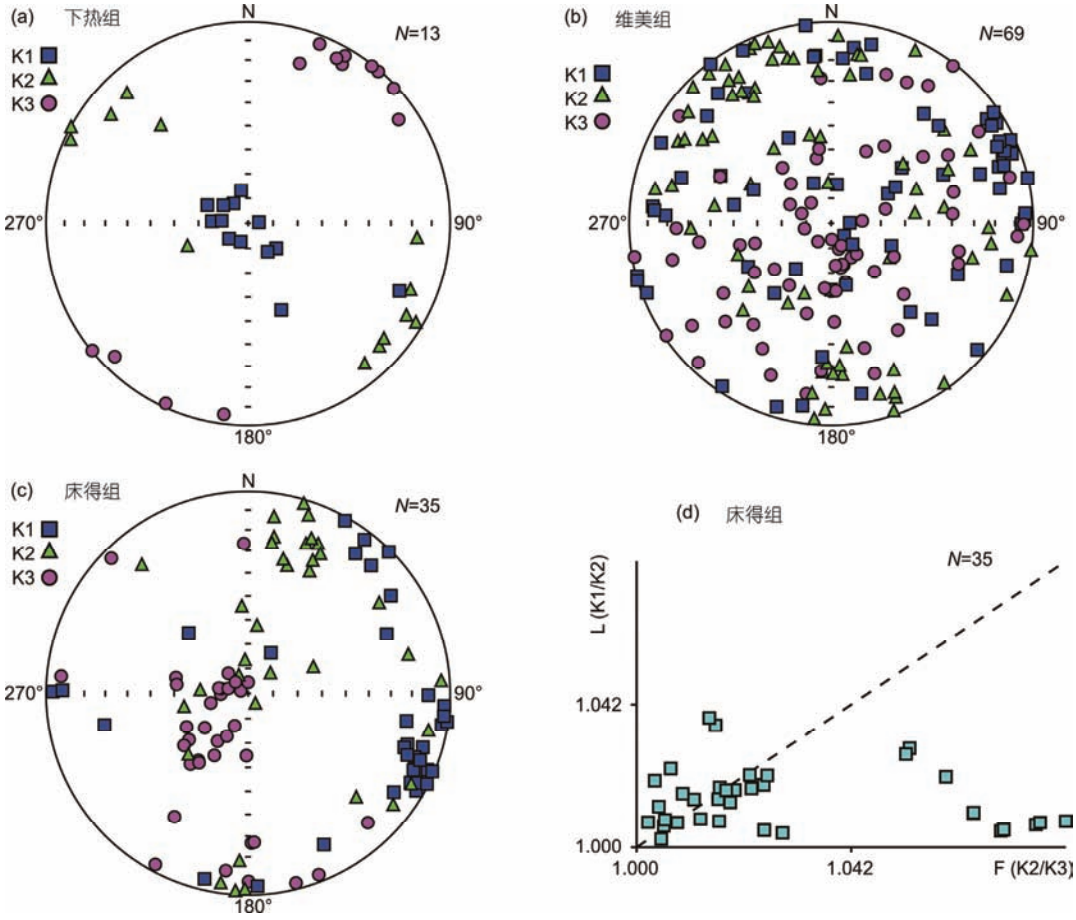

图 2 床得剖面各组样品的磁化率各向异性等面积投影图(地层坐标系)以及床得组样品的Flinn图解. *N*, 测试样品的数量; L, 线理; F, 面理

Figure 2 The anisotropy of magnetic susceptibility (AMS) data of samples from different formations of the Chuangde section (stratigraphic coordinates) and the F-L diagram of samples from the Chuangde Formation. *N*, number of samples measured; L, lineation; F, foliation

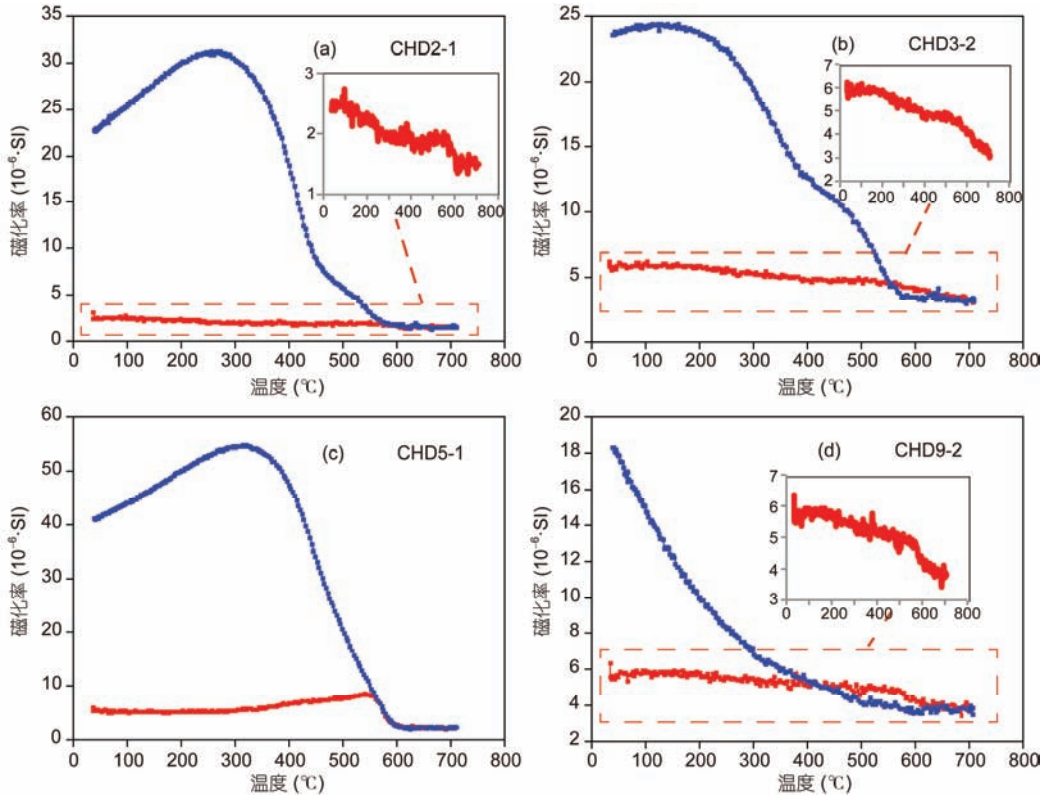

图 3 床得组代表性样品磁化率-温度曲线

Figure 3 Temperature-dependent low-field magnetic susceptibility curves of representative specimens from the Chuangde Formation

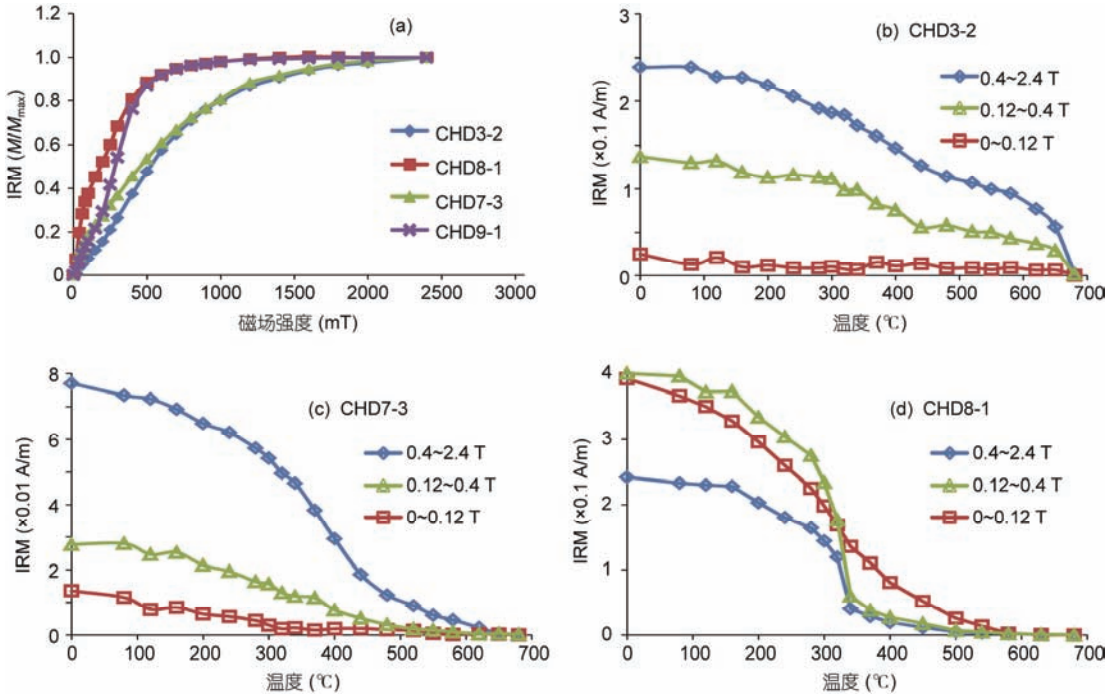

图 4 床得组代表性样品等温剩磁获得曲线(a)和三轴等温剩磁热退磁曲线((b)~(d)). IRM, 等温剩磁; M/M_{max}, 归一化的等温剩磁强度

Figure 4 Normalized isothermal remanent magnetization (IRM) acquisition curves (a) and thermal demagnetization of the composite IRM (b)–(d) that was acquired sequentially along three orthogonal axes; M/M_{max}, normalized isothermal remanent magnetization

样品中存在以中高矫顽力为主的携磁矿物(如赤铁矿), 同时也可能存在少量低矫顽力的携磁矿物(如磁铁矿). 三轴等温剩磁热退磁实验结果也分为两类: (1) 硬磁和中磁成分的解阻温度均在680℃, 表明主要携磁矿物为赤铁矿(图4(b)); (2) 硬磁和中磁成分在300~470℃时剩磁强度明显下降, 且中磁和软磁成分在580℃出现拐点而硬磁成分在650℃左右出现拐点, 指示同时含有赤铁矿、磁铁矿(图4(c)). 个别样品中, 软磁成分贡献占主导, 其解阻温度为580℃, 指示磁铁矿为主要的携磁矿物, 贡献较小的硬磁和中磁成分强度在~350℃明显下降(图4(d)), 指示可能存在铁硫化物. 岩石磁学实验结果表明, 床得组样品的携磁矿物以磁铁矿或赤铁矿为主, 部分样品同时含有这两种携磁矿物.

3.3 退磁结果

大约95%的样品进行了热退磁实验, 5%的样品进行了交变退磁实验. 根据退磁数据质量, 可以将样品分为A, B, C三类. A类样品退磁结果稳定, ChRM高温段明显趋向于原点, 且可分离出低温和高温两个分量(图5(a)~(e), 表S1和S2). 其中, 低温分量一般在250~300℃或20 mT左右被完全分离, 高温分量通常在300℃至540~580℃或20~100 mT之间分离, 偏角SE或S, 倾角为正(图5(a), (c), (d)); 三个样品的高温分量在480~620℃之间分离, 偏角NW, 倾角为负(图5(b)). B类样品的高温分量不稳定, 直至680℃或100 mT也没有趋向原点(图5(f)), 无法确定特征剩磁分量. 其低温分量能够在300℃或30 mT之前被分离出来. C类样品的退磁轨迹不稳定, 无法分离出低温分

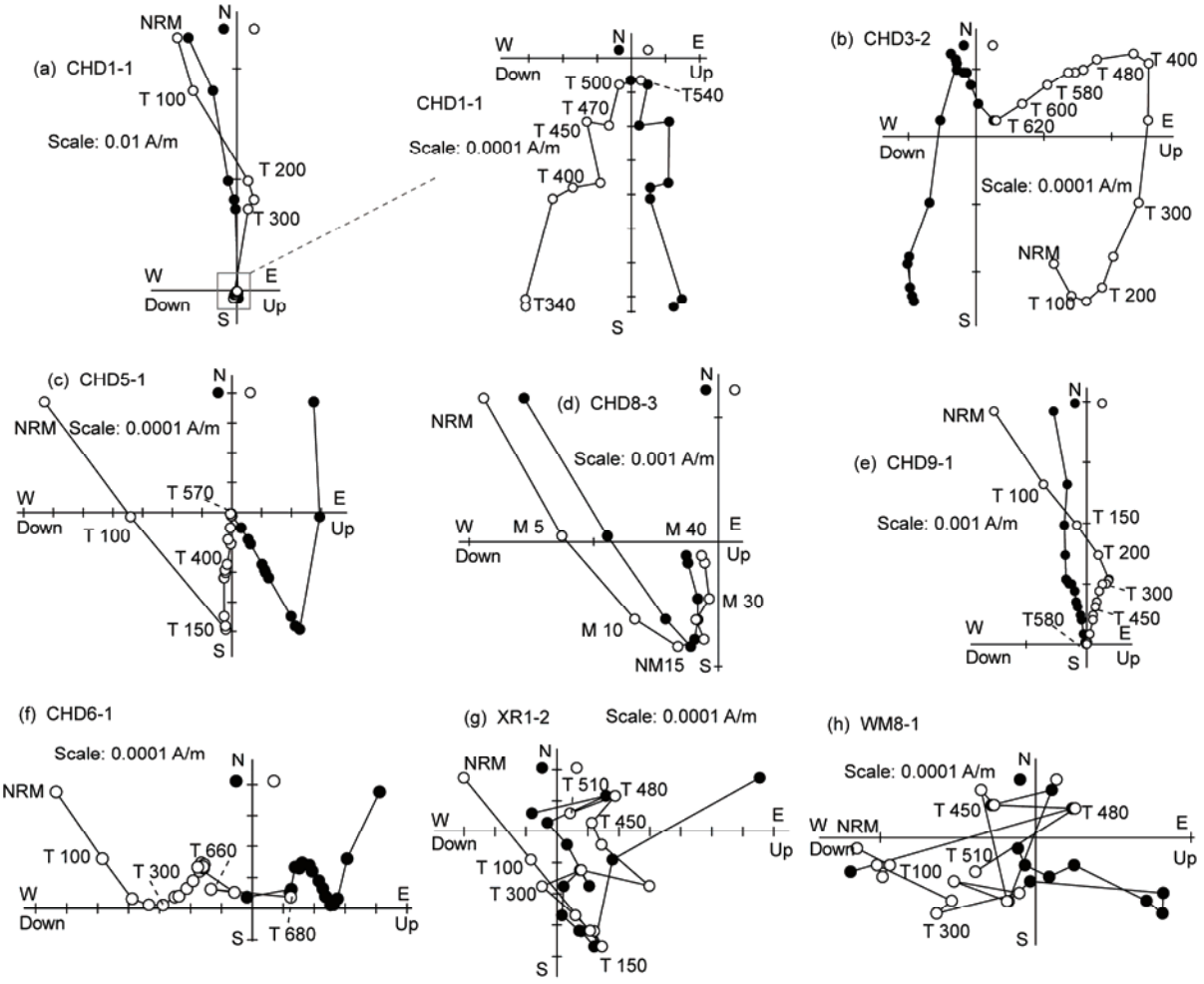

图 5 代表性样品逐步退磁结果(地理坐标系). T(M)代表热退磁(交变退磁)步骤; 实心点(空心点)代表退磁步骤在水平面(垂直面)上的投影

Figure 5 Representative orthogonal projection of paleomagnetic demagnetization data (geographic coordinates). T and M, thermal and alternating field demagnetization steps; the solid/open circles represent the projections onto the horizontal/vertical planes, respectively

量和高温分量(图5(g)~(h)). 床得组46个样品中35个样品的退磁结果属于A类, 11个样品的退磁结果为B类. 下热组和维美组70%以上样品的退磁结果属于C类, 30%的样品退磁结果属于B类, 无法分离出稳定的特征剩磁分量(ChRM).

床得组样品分离出的低温分量在地理坐标系下的平均方向是: D_g=357.4°, I_g=46.8°, n=40, κ=17.2, α_{95}=5.6°(图6(a)); 地层坐标下的平均方向是: D_s=160.3°, I_s=62.3°, n=40, κ=10.4, α_{95}=7.4°(图6(b)). 比较两者的κ值和α_{95}可知, 低温分量在地理坐标系下相对更为集中, 并且其平均方向与现代地磁场方向(D=0.2°, I=45.1°)非常接近, 是现代地磁场中获得的黏滞剩磁. 对于床得组样品的高温分量, A类样品的高温分量在300℃之后随着温度的逐步升高而呈线性趋向原点, 代表特征剩磁的方向; B类样品主要来自采样点CHD4和CHD6, 因此, 在这两个采样点上未获得特征剩磁. 其余的7个采样点的样品均能分离出稳定的特征剩磁. 其中2个采样点的特征剩磁表现为反极性, 5个采样点的特征剩磁表现为正极性(表1). 由于正反极性结果并存, 可用这7个采样点所有A类样品的高温剩磁分量(n=35)作倒转检验. 结果表明, 在95%置信水平下γ_0=7.6°< γ_c=13.0°, 即通过了C级倒转检验[48]. 因此, 这7个采点样品所携带的特征剩磁很可能代表了原生剩磁. 对这7个采样点所有A类样品的高温分量进行Fisher统计, 获得地理坐标系下的平均方向为: D_g=157.9°, I_g=16.4°, n=35, κ=15.6, α_{95}=6.3°(图6(c)); 地层坐标系下的平均方向为: D_s=152.0°, I_s=–52.9°, n=35, κ=18.0, α_{95}=5.9°(图6(d)). 对应的古地磁极为λ=–65.7°, φ=197.6°, dp=5.6°, dm=8.2°. 通过计算, 得到参考点(28.0°N, 88.5°E)处的古

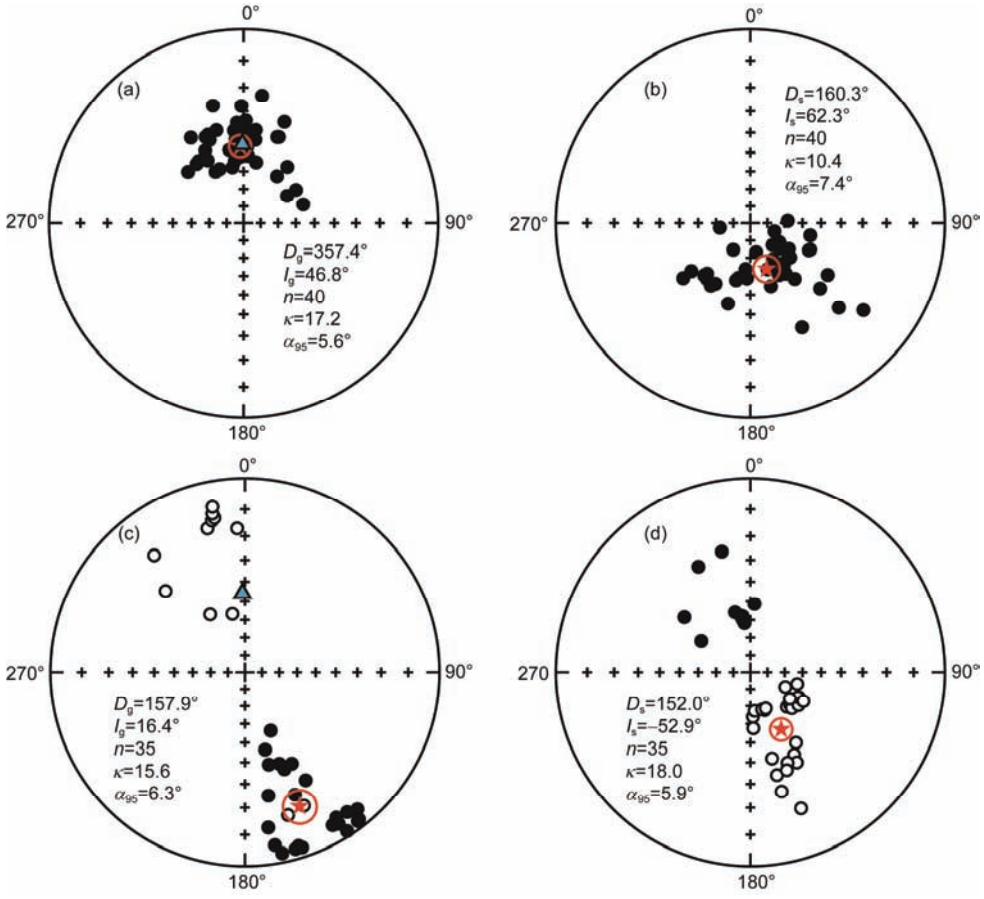

图 6 床得组样品的低温分量((a), (b))和高温分量((c), (d))赤平投影图. (a), (c) 地理坐标系; (b), (d) 地层坐标系; 五角星表示平均方向; 实心(空心)点为下(上)半球投影; 三角形表示现代地磁场方向

Figure 6 Equal-area stereonet projections of the low-temperature components and high-temperature components of representative specimens from the Chuangde Formation before ((a), (c)) and after ((b), (d)) tilt correction. The stars represent the mean directions; the solid/open circles represent downward/upward inclinations; the triangles represent the present-day Earth's magnetic field

表 1　床得组各采样点特征剩磁平均方向[a)]

Table 1　Mean directions of the ChRMs of sites from the Chuangde Formation

采样点	岩性	倾向/倾角	*n*/*N*	极性	地理坐标		地层坐标			
					D_g(°)	I_g(°)	D_s(°)	I_s(°)	κ	α_{95}(/SA) (°)
CHD9	粉砂质灰岩	165°/70°	6/6	反	349.3	–12.6	352.8	57.1	268.0	4.1
CHD8	粉砂质灰岩	165°/70°	7/7	正	158.2	37.9	158.7	–31.8	63.3	7.6
CHD7	粉砂质灰岩	165°/70°	6/7	正	166.5	5.0	168.5	–65.0	228.5	4.4
CHD6	砂质灰岩	165°/70°	–/3	–	–	–	–	–	–	–
CHD5	砂质灰岩	165°/70°	8/8	正	145.5	4.3	124.7	–59.1	414.5	2.7
CHD4	泥灰岩	165°/70°	–/5	–	–	–	–	–	–	–
CHD3	泥灰岩	165°/81°	4/6	反	326.4	–38.7	326.2	39.2	14.3	25.2
CHD2	灰岩	185°/67°	2/2	正	159.8	–15.4	108.2	–65.1	276.0	/15.1
CHD1	灰岩	185°/67°	2/2	正	163.5	22.8	159.0	–39.8	112.0	/23.8
床得组特征剩磁平均方向(A类样品)										
			35/46		157.9	16.4			15.6	6.3
							152.0	–52.9	18.0	5.9

a) *n*/*N*, 参与统计的样品数/退磁样品数; D_g, I_g, 地理坐标系下磁偏角和磁倾角; D_s, I_s, 地层坐标系下磁偏角和磁倾角; κ, 精度参数估计值; α_{95}, 95%置信圆锥半顶角; /SA, 夹角; d*p*/d*m*=5.6°/8.2°, 古地磁极置信椭圆的纬/经向半径; 古地磁极(–65.7°N, 197.6°E), 古纬度为–33.1°±5.6°

纬度为南纬33.1°±5.6°.

4　讨论

4.1　床得组特征剩磁的年代及极性

据Wan等人[40]对该剖面床得组微体古生物特征的分析, 床得组红层底部和顶部地层分别记录了浮游有孔虫*D. asymetrica*和*G. aegyptiaca*的首现, 其时代为白垩纪Santonian晚期至Campanian中期. 因此, 根据生物地层的约束, 可将床得组地层的年龄跨度限定于~86.3~74.0 Ma之间[49]. 床得组样品的特征剩磁既有正极性, 也有反极性, 且通过了倒转检验. 岩石磁学结果表明磁铁矿和赤铁矿为主要载磁矿物. 另外, 磁化率各向异性结果显示为沉积类型组构. 而且, 岩相薄片分析表明床得组岩石新鲜, 后期蚀变作用弱[39]. 综合古地磁、岩石磁学和岩相学结果表明, 床得组的特征剩磁很可能为原生剩磁, 其年代范围为86.3~74.0 Ma. 床得组特征剩磁在地层坐标系下的平均方向为: D_s=152.0°, I_s=–52.9°, κ=18.0, α_{95}=5.9°. 如果该方向为反极性, 则表明研究区经历了~30°逆时针旋转, 其古纬度为北纬~33.1°. 由于特提斯喜马拉雅在68±3 Ma时位于南纬6.0°±4.4°[12](参考点: 28.0°N, 88.5°E), 这意味着特提斯喜马拉雅需要先北向再南向漂移约3000 km. 这样的演化与地质事实不符. 而且, 拉萨地块~80 Ma时位于北纬~20°[7]. 如果特提斯喜马拉雅~80 Ma时处于北纬~33.1°, 二者应该已经发生了碰撞. 这明显与~59 Ma的初始碰撞时间相悖[11]. 因此, 床得组特征剩磁的平均方向应该为正极性, 表明研究区自~80 Ma以来经历了绕垂直轴~150°顺时针旋转, 在~80 Ma时处于南半球. 对不同采样点的古地磁结果, 磁倾角为负的采样点层位记录了磁场的正极性期, 反之, 磁倾角为正的则记录了磁场的反极性期. 虽然床得组的古地磁结果不足以建立精细的磁性地层年代, 但由于床得组为深海沉积, 沉积速率缓慢且相对稳定, 其古地磁结果所揭示的正、反地磁极性序列与国际标准地磁极性年表[50]中86.3~74.0 Ma之间的地磁极性序列总体一致(图7).

4.2　特提斯喜马拉雅与印度板块的关系

早白垩世时期, 由特提斯喜马拉雅和印度板块构成的大印度板块作为一个整体一起从冈瓦纳大陆裂解出来并开始向北漂移[51,52]. 因此, 二者在向北漂移的过程中是否发生过分离、分离的具体时间等科学问题, 可以通过对比它们同时代的古地磁结果来分析. 对印度板块而言, 前人已经做了大量的古地磁研究并获得了印度板块的视极移曲线[53], 以印度板块和特提斯喜马拉雅的边界点28.0°N, 88.5°E为参考点,

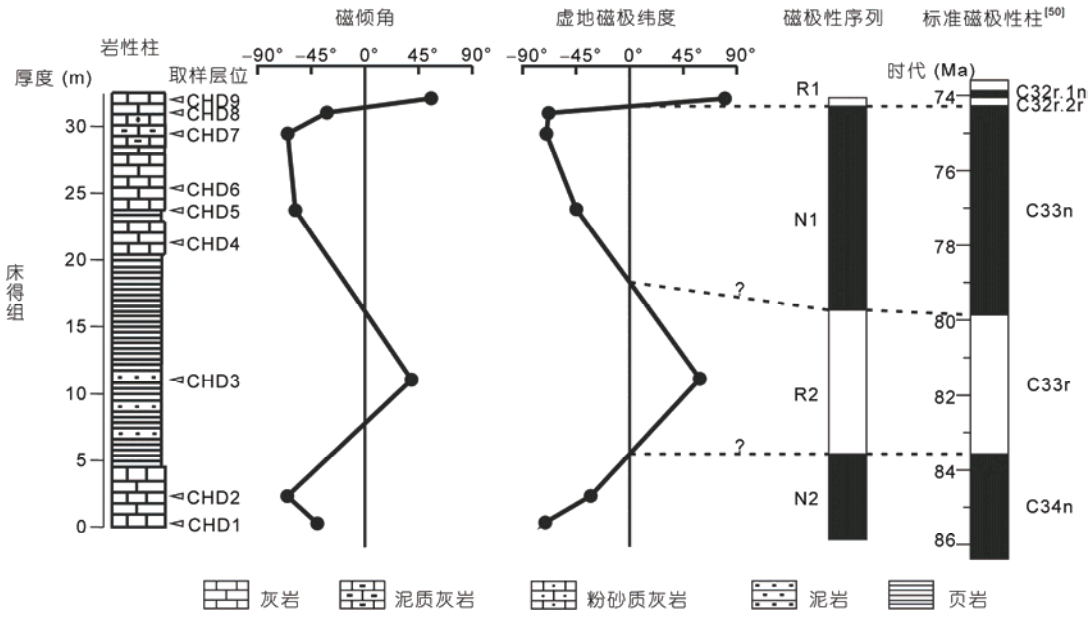

图 7 床得组岩性柱、磁极性序列与国际标准磁极性年代对比

Figure 7 Magnetostrtigraphy of the Chuangde Formation and its tentative correlation with the geomagnetic polarity time scale

根据印度板块的视极移曲线，可以计算出其北缘不同时期所处的古纬度及磁偏角(指示旋转)(表S3，图8). 同样，根据从特提斯喜马拉雅获得的中生代以来的古地磁结果，也可以计算出特提斯喜马拉雅南缘不同时期所处的古纬度及旋转历史(表S3，图8). 在旋转对古纬度估计影响较小的情况下，二者之间在同时代是否存在古纬度差异可以用来判别特提斯喜马拉雅是否与印度板块发生了分离.

如前所述，床得组特征剩磁很可能为原生剩磁，年代为约86.3~74 Ma，其平均方向为: D_s=152.0°, I_s=−52.9°, κ=18.0, α_{95}=5.9°，且为正极性. 该结果表明，特提斯喜马拉雅南缘在80.1±6.2 Ma时处于南纬33.1°±5.6°，并经历了~150°的顺时针旋转. 由于大印度板块从冈瓦纳分离以来主要经历了逆时针旋转[6,12,21,25] (图8，磁偏角)，所观察到的~150°顺时针旋转与整个块体总体的逆时针旋转不协调. 据Hu 等人[39]和Chen等人[54]对床得组的岩相学研究及沉积环境分析，床得组页岩与下伏甲不拉组页岩是整合连续的，沉积环境一致，均为深水且可能在碳酸盐补偿深度(CCD)面之下的沉积环境. 但床得组红色灰岩最初形成于远洋深水陆棚或者大陆上斜坡，是通过滑移或滑塌进入大陆斜坡外的深水盆地的. 因此，本研究所得到的~150°顺时针旋转可能是由于形成于斜坡相的床得组红色灰岩在滑移或滑塌进入到深水盆地过程中岩块的局部旋转所引起的. 由于岩块的局部旋转不会影响磁倾角，磁倾角仍然可以用来估算特提斯喜马拉雅的古纬度. 根据磁倾角计算，特提斯喜马拉雅的南缘在80.1±6.2 Ma时处于南纬33.1°±5.6°. 而印度板块北缘在~80 Ma的古纬度为南纬31.2°±2.9°[53]. 两者在~80 Ma时的古纬度差为1.9°±6.3°. 印度板块和特提斯喜马拉雅~80 Ma以来的逆时针旋转约5°~15°(图8，磁偏角)，其对古纬度差估计的影响很小(以10°计，其对纬度差估计的影响仅为10°×cos[(180°−10°)/2]=0.87°). 因此，两者在~80 Ma时所处的古纬度在误差范围内是一致的. 这一结果表明，特提斯喜马拉雅至少在~80 Ma时与印度板块仍然是一个整体，并没有与印度板块分离(图8).

早白垩世古地磁数据显示，特提斯喜马拉雅与印度板块在~130和~120 Ma的古纬度基本一致(图8)[20,21,25]，而且在早白垩世发生了不同幅度的逆时针旋转(图8，磁偏角). 由于特提斯喜马拉雅早白垩世以来经历了~90°的逆时针旋转[20,21]，与印度板块相同的古纬度并不一定指示二者之间没有发生分离. 结合其他地质证据来看，由于二者之间并不存在一个被动陆缘沉积盆地[55]，而且二者晚白垩世以来旋转的性质和幅度总体一致(图8)，特提斯喜马拉雅与印度板块在白垩世很可能是作为一个整体经历了逆时针旋转和北向漂移的. 因此，至少在80 Ma之前，

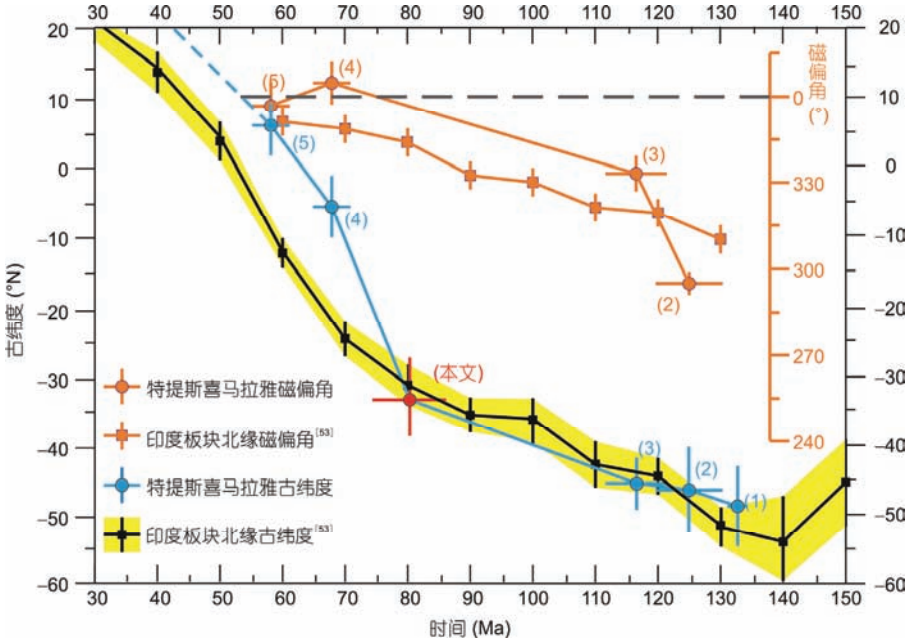

图 8 特提斯喜马拉雅南缘与印度板块北缘古纬度对比(以 28°N, 88.5°E为参考点). 阴影区域和竖直短线表示纬度误差范围或磁偏角误差范围; 水平短线表示时间范围. 小括号内数字表示前人已获得的古地磁数据: (1) Yang等人[20]; (2) Ma等人[21]; (3) Klootwijk等人[25]; (4) Patzelt等人[12]; (5) Patzelt等人[12]、Yi等人[6]、Yang等人[20]

Figure 8 Comparison of the paleolatitudes of Tethyan Himalaya and India (reference point: 28°N, 88.5°E). The shaded area and vertical bars indicate the uncertainties of the estimated paleolatitudes or declinations; the horizontal bars represent the uncertainties in ages. The numbers in brackets indicate sources of paleomagnetic data. (1) Yang et al.[20]; (2) Ma et al.[21]; (3) Klootwijk et al.[25]; (4) Patzelt et al.[12]; (5) Yi et al.[6], Patzelt et al.[12], Yang et al.[20]

特提斯喜马拉雅与印度板块很可能一直是一个整体, 并没有发生分离.

然而, 从特提斯喜马拉雅岗巴地区获得的白垩纪末期古地磁数据表明, 岗巴地区在68±3 Ma时的古纬度为–6.0°±4.4°[12]; Patzelt等人[12]和Yi等人[6]从岗巴地区获得了古新世的古地磁结果, Yang等人[20]对这些结果重新统计获得的古地磁极为λ=69.6°, φ=272.5°, A_{95}=1.7°, 用该古地磁极计算得到岗巴地区在59±3 Ma时的古纬度为7.6°±1.7°(参考点: 28°N, 88.5°E). 这与同时代印度板块北缘的纬度差分别达到了16.2°±5.0°和18.7°±2.8°(图8, 印度板块北缘的古纬度分别由70~60和60~50 Ma漂移的平均速度推算). 另一方面, 尼泊尔低喜马拉雅始新世中期Bhainskati组已经开始接受特提斯喜马拉雅的沉积[56], 这说明印度克拉通与特提斯喜马拉雅最晚在始新世中期(45 Ma)已经成为一体. 如果特提斯喜马拉雅在晚白垩世(74 Ma之后)确实与印度北缘发生分离, 那么两个块体须在45 Ma之前聚合, 即意味着要在30 Myr年内(74~45 Ma)完成~1700 km的裂离又聚合的整个过程, 而这样的过程很难用板块构造解释. 就现有的地质资料而言, 目前尚缺乏晚白垩世裂解的地质证据: (1) 印度北缘没有晚白垩世裂解构造和裂谷火山作用; (2) 在定日-岗巴地区白垩纪末期-古新世早期遮普热山坡组和基堵拉组发现了高钛尖晶石, 被解释为来源于印度克拉通德干玄武岩[57]; (3) 遮普热山坡组和基堵拉组整体表现为古水深向上变浅的地层序列[58,59], 与裂解作用导致的古水深变深的趋势相反. 另一方面, 来自特提斯喜马拉雅的晚白垩世-早古近纪的古地磁数据还较少, 且可靠性还有待于进一步提高. 鉴于特提斯喜马拉雅与亚洲大陆的初始碰撞时间为~59 Ma[11], 结合床得组大洋红层的古地磁结果, 本研究认为, 特提斯喜马拉雅与亚洲大陆的碰撞就是印度-亚洲大陆的碰撞.

5 结论

本文对藏南江孜地区床得剖面侏罗系-上白垩统地层开展了古地磁研究, 逐步热退磁和交变退磁结果显示侏罗系下热组和维美组样品未能分离出稳定的特征剩磁, 而上白垩统床得组样品中记录了稳定且通过倒转检验的特征剩磁. 结合沉积学及岩石磁

学结果, 床得组特征剩磁很可能为原生剩磁. 根据生物地层约束, 床得组剩磁获得的时间为86.3~74.0 Ma. 床得组特征剩磁的平均方向为D_s=152.0°, I_s=–52.9°, κ=18.0, α_{95}=5.9°. 该数据表明, 特提斯喜马拉雅在晚白垩世(80.1±6.2 Ma)所处的古纬度为南纬33.1°±5.6°, 与同时代的印度板块北缘古纬度一致(参考点28.0°N, 88.5°E). 说明二者至少在~80 Ma之前仍然是一个块体, 并没有分离. 床得组的古地磁结果为探讨印度板块与亚洲大陆的碰撞过程提供了新约束.

致谢 感谢南京大学马丽凤在野外工作中的帮助. 感谢审稿人的宝贵意见, 感谢中国科学院南海海洋研究所谈晓冬研究员和中国地质大学(北京)陈曦博士分享在构造磁学和白垩纪大洋红层研究方面的宝贵经验. 香港大学Jason R. Ali博士对英文摘要做了修饰润色, 在此一并表示感谢.

参考文献

1 Besse J, Courtillot V, Pozzi J P, et al. Paleomagnetic estimates of crustal shortening in the Himalayan thrusts and Zangbo suture. Nature, 1984, 311: 621–626
2 Jaeger J J, Courtillot V, Tapponnier P. Paleontological view of the ages of the Deccan Traps, the Cretaceous/Tertiary boundary and the India-Asia collision. Geology, 1989, 17: 316–319
3 Aitchison J C, Mcdermid I R C, Ali J R, et al. Shoshonites in southern Tibet record Late Jurassic rifting of a Tethyan Intraoceanic island arc. J Geol, 2007, 115: 197–273
4 Najman Y, Appel E, Boudagher-Fadel M, et al. Timing of India-Asia collision: Geological, biostratigraphic, and palaeomagnetic constraints. J Geophys Res, 2010, 115: B12416, doi: 10.1029/2010JB007673
5 Tan X, Gilder S, Kodama K P, et al. New paleomagnetic results from the Lhasa block: Revised estimation of latitudinal shortening across Tibet and implications for dating the India-Asia collision. Earth Planet Sci Lett, 2010, 293: 396–404
6 Yi Z Y, Huang B C, Chen J S, et al. Paleomagnetism of early Paleogene marine sediments in southern Tibet, China: Implications to onset of the India-Asia collision and size of Greater India. Earth Planet Sci Lett, 2011, 309: 153–165
7 Van Hinsbergen D J, Lippert P C, Dupont-Nivet G, et al. Greater India Basin hypothesis and a two-stage Cenozoic collision between India and Asia. Prod Natl Acad Sci USA, 2012, 109: 7659–7664
8 Chen J S, Huang B C, Sun L S. New constraints to the onset of the India-Asia collision: Paleomagnetic reconnaissance on the Linzizong Group in the Lhasa Block, China. Tectonophysics, 2010, 489: 189–209
9 Ma Y M, Yang T S, Yang Z Y, et al. Paleomagnetism and U-Pb zircon geochronology of lower Cretaceous lava flows from the western Lhasa terrane: New constraints on the India-Asia collision process and intracontinental deformation within Asia. J Geophys Res-Solid Earth, 2014, 119: 7404–7424
10 Decelles P G, Kapp P, Gehrels G E, et al. Paleocene-Eocene foreland basin evolution in the Himalaya of southern Tibet and Nepal: Implications for the age of initial India-Asia collision. Tectonics, 2014, 33: 824–849
11 Hu X M, Garzanti E, Moore T, et al. Direct stratigraphic dating of India-Asia collision onset at the Selandian (middle Paleocene, 59±1 Ma). Geology, 2015, 43: 859–862
12 Patzelt A, Li H M, Wang J D, et al. Palaeomagnetism of Cretaceous to Tertiary sediments from southern Tibet: Evidence for the extent of the northern margin of India prior to the collision with Eurasia. Tectonophysics, 1996, 259: 259–284
13 Sun Z M, Pei J L, Li H B, et al. Palaeomagnetism of late Cretaceous sediments from southern Tibet: Evidence for the consistent palaeolatitudes of the southernmargin of Eurasia prior to the collision with India. Gondwana Res, 2012, 21: 53–63
14 Meng J, Wang C S, Zhao X X, et al. India-Asia collision was at 24°N and 50 Ma: Palaeomagnetic proof from southernmost Asia. Sci Rep, 2012, 2: 925
15 Chen W W, Yang T S, Zhang S H, et al. Paleomagnetic results from the Early Cretaceous Zenong Group volcanic rocks, Cuoqin, Tibet, and their paleogeographic implications. Gondwana Res, 2012, 22: 461–469
16 Van der Voo R, Spakman W, Bijwaard H. Tethyan subducted slabs under India. Earth Planet Sci Lett, 1999, 184: 1–9
17 Aitchison J C, Badengzhu, Davis A M, et al. Remnants of a Cretaceous intra-oceanic subduction system within the Yarlung-Zangbo suture (southern Tibet). Earth Planet Sci Lett, 2000, 183: 231–244
18 Lippert P C, Douve J J, Van Hinsbergen, et al. Early Cretaceous to present latitude of the central proto-Tibetan Plateau: A paleomagnetic synthesis with implications for Cenozoic tectonics, paleogeography, and climate of Asia. Geol Soc Am Spec Paper, 2014, 507, doi: 10.1130/2014.2507(01)

19 Jagoutz O, Royden L, Holt A F, et al. Anomalously fast convergence of India and Eurasia caused by double subduction. Nat Geosci, 2015, 8: 475–478
20 Yang T S, Ma Y M, Bian W W, et al. Paleomagnetic results from the early Cretaceous Lakang Formation lavas: Constraints on the paleolatitude of the Tethyan Himalaya and the India-Asia collision. Earth Planet Sci Lett, 2015, 428: 120–133
21 Ma Y M, Yang T S, Bian W W, et al. Early Cretaceous paleomagnetic and geochronologic results from the Tethyan Himalaya: Insights into the Neotethyan paleogeography and the India-Asia collision. Sci Rep, 2016, 6: 21605
22 Gansser A. The significance of the Himalayan suture zone. Tectonophysics, 1980, 62: 37–52
23 Yin A, Harrison M. Geologic evolution of the Himalayan-Tibetan orogen. Annu Rev Earth Planet Sci, 2000, 28: 211–280
24 Hodges K V. Tectonics of the Himalaya and southern Tibet from two perspectives. Geol Soc Am Bull, 2000, 112: 324–350
25 Klootwijk C T, Bingham D K. The extent of Greater India, III. Palaeomagnetic data from the Tibetan sedimentary series, Thakkhola region, Nepal Himalaya. Earth Planet Sci Lett, 1980, 51: 381–405
26 Hu X M, Jansa L B, Wang C S. Upper Jurassic-Lower Cretaceous stratigraphy in south-eastern Tibet: A comparison with the western Himalayas. Cretac Res, 2008, 29: 301–315
27 Li X H, Wang C S, Wan X Q, et al. Verification of stratigraphical sequence and classification of the Chuangde Section of Gyangze, South Tibet (in Chinese). J Stratingr, 1999, 4: 303–309 [李祥辉, 王成善, 万晓樵, 等. 藏南江孜县床得剖面侏罗-白垩纪地层层序及地层划分. 地层学杂志, 1999, 4: 303–309]
28 Huang W T, van Hinsbergen D J J, Dekkers M J, et al. Paleolatitudes of the Tibetan Himalaya from primary and secondary magnetizations of Jurassic to Lower Cretaceous sedimentary rocks. Geochem Geophys Geosyst, 2015, 16: 77–100
29 Tong Y B, Yang Z Y, Zheng L D, et al. Early Paleocene paleomagnetic results from southern Tibet, and tectonic implications. Int Geol Rev, 2008, 50: 546–562
30 Liebke U, Appel E, Ding L, et al. Age constraints on the India-Asia collision derived from secondary remanences of Tethyan Himalayan sediments from the Tingri area. J Asian Earth Sci, 2013, 62: 329–340
31 Appel E, Muller R, Widder W. Palaeomagnetic results from the Tibetan sedimentary series of the Manang area, north central Nepal. Geophys J Int, 1991, 104: 255–266
32 Liu G H, Einsele G. Sedimentary history of the Tethyan basin in the Tibetan Himalayas. Geol Rundsch, 1994, 83: 32–61
33 Garzanti E. Stratigraphy and sedimentary history of the Nepal Tethys Himalaya passive margin. J Asian Earth Sci, 1999, 17: 805–827
34 Zhu D C, Pan G T, Mo X X, et al. Permian to Cretaceous volcanic activities in the central segment of the Tethyan Himalayas (I): Distribution characteristics and significance (in Chinese). Geol Bull China, 2004, 23: 645–654 [朱弟成, 潘桂棠, 莫宣学, 等. 藏南特提斯喜马拉雅带中段二叠纪一白垩纪的火山活动(I): 分布特点及其意义. 地质通报, 2004, 23: 645–654]
35 Yin A. Cenozoic tectonic evolution of the Himalayan orogen as constrained by along-strike variation of structural geometry, exhumation history, and foreland sedimentation. Earth-Sci Rev, 2006, 76: 1–131
36 Wu H R. Late Cretaceous to Early Tertiary (?) strata in Gyangze area, Southern Tibet (in Chinese). J Stratigr, 1987, 11: 147–149 [吴浩若. 西藏南部江孜地区晚白垩世晚期及早第三纪(?)地层. 地层学杂志, 1987, 11: 147–149]
37 Hu X M. Sedimentary geology of Cretaceous in Southern Tibet, and the Upper Cretaceous oceanic redbeds (in Chinese). Doctor Dissertation. Chengdu: Chengdu University of Technology, 2002 [胡修棉. 藏南白垩系沉积地质与上白垩统海相红层. 博士学位论文. 成都: 成都理工大学, 2002]
38 Chen X, Wang C S, Hu X M, et al. Petrology and evolution history from Late Jurassic to Paleogene of Gyangze basin, Southern Tibet (in Chinese). Acta Petrol Sin, 2008, 24: 616–625 [陈曦, 王成善, 胡修棉, 等. 西藏南部江孜盆地上侏罗统至古近系沉积岩石学特征与盆地演化. 岩石学报, 2008, 24: 616–625]
39 Hu X M, Wang C S, Li X H, et al. Upper Cretaceous oceanic red beds in southern Tibet: Lithofacies, environments and colour origin. Sci China Ser D-Earth Sci, 2006, 49: 785–795
40 Wan X Q, Lamolda M A, Si J L, et al. Foraminiferal stratigraphy of Late Cretaceous red beds in southern Tibet. Cretac Res, 2005, 26: 43–48
41 Thébault E, Finlay C C, Beggan C D, et al. International Geomagnetic Reference Field: The 12th generation. Earth Planets Space, 2015, 67: 79
42 Zijderveld J D A. Ac demagnetization of rocks: Analysis of results. In: Collinson D W, Creer K M, Runcorn S K, eds. Methods in Paleomagnetism. Amsterdam: Elsevier, 1967. 254–286
43 Kirschvink J L. The least-squares line and plane and the analysis of palaeomagnetic data. Geophys J Int, 1980, 62: 699–718
44 Fisher R A. Dispersion on a sphere. Proc R Soc A-Math Phys Eng Sci, 1953, 217: 295–305
45 Enkin R J. Formation et déformation de l'Asie depuis la fin de lère primaire: Les apports de l'étude paléomagnétique des formations secondaires de Chine du Sud. Doctor Dissertation. Paris: Univ de Paris 7, 1990

46 Cogné J P. PaleoMac: A MacintoshTM application for treating paleomagnetic data and making plate reconstructions. Geochem Geophys Geosyst, 2003, 4: 1–8
47 Liu Q S, Deng C L, Yu Y, et al. Temperature dependence of magnetic susceptibility in an argon environment: Implications for pedogenesis of Chinese loess/paleosols. Geophys J Int, 2005, 1: 102–112
48 McFadden P, McElhinny M. Classification of the reversal test in palaeomagnetism. Geophys J Int, 1990, 103: 725–729
49 Ogg J G, Hinnov L A. Cretaceous. In: Gradstein F M, Ogg J G, Schmitz M, et al., eds. The Geologic Time Scale 2012. Amsterdam: Elsevier, 2012. 793–853
50 Ogg J G. Geomagnetic polarity time scale. In: Gradstein F M, Ogg J G, Schmitz M, et al., eds. The Geologic Time Scale 2012. Amsterdam: Elsevier, 2012. 85–113
51 Zhu D C, Chung S L, Mo X X, et al. The 132 Ma Comei-Bunbury large igneous province: Remnants identified in present-day southeastern Tibet and southwestern Australia. Geology, 2009, 37: 583–586
52 Hu X M, Jansa L, Chen L, et al. Provenance of Lower Cretaceous Wölong volcaniclastics in the Tibetan Tethyan Himalaya: Implications for the final breakup of Eastern Gondwana. Sediment Geol, 2010, 223: 193–205
53 Torsvik T H, van der Voo R, Preeden U, et al. Phanerozoic polar wander, palaeogeography and dynamics. Earth-Sci Rev, 2012, 114: 325–368
54 Chen X, Wang C S, Kuhnt W, et al. Lithofacies, microfacies and depositional environments of Upper Cretaceous Oceanic red beds (Chuangde Formation) in southern Tibet. Sediment Geol, 2011, 235: 100–110
55 Hu X M, Garzanti E, Wang J, et al. The timing of India-Asia collision onset: Facts, theories, controversies. Earth-Sci Rev, 2016, 160: 264–299
56 Garzanti E, Hu X M. Latest Cretaceous Himalayan tectonics: Obduction, collision or deccan-related uplift? Gondwana Res, 2015, 28: 165–178
57 Willems H, Zhou Z, Zhang B, et al. Stratigraphy of the Upper Cretaceous and Lower Tertiary strata in the Tethyan Himalayas of Tibet (Tingri area, China). Geol Rundsch, 1996, 85: 723–754
58 Hu X M, Sinclair H D, Wang J G, et al. Late Cretaceous-Palaeogene stratigraphic and basin evolution in the Zhepure Mountain of southern Tibet: Implications for the timing of India-Asia initial collision. Basin Res, 2012, 24: 520–543
59 DeCelles P G, Gehrels G E, Najman Y, et al. Detrital geochronology and geochemistry of Cretaceous-Early Miocene strata of Nepal: Implications for timing and diachroneity of initial Himalayan orogenesis. Earth Planet Sci Lett, 2004, 227: 313–330

补充材料

表 S1 床得组低温剩磁方向
表 S2 床得组高温剩磁方向
表 S3 特提斯喜马拉雅南缘与印度板块北缘古纬度对比(以 28°N，88.5°E 为参考点)

本文以上补充材料见网络版 csb.scichina.com. 补充材料为作者提供的原始数据, 作者对其学术质量和内容负责.

Summary for “藏南床得剖面古地磁结果对印度-亚洲碰撞方式的约束”

Paleomagnetic results from Jurassic-Cretaceous strata in the Chuangde area of southern Tibet constrain the nature and timing of the India-Asia collision system

ZHANG BoXing, LI YongXiang* & HU XiuMian

State Key Laboratory for Mineral Deposit Research, School of Earth Sciences and Engineering, Nanjing University, Nanjing 210023, China
* Corresponding author, E-mail: yxli@nju.edu.cn

The Tethyan Himalaya sits between the India craton and the Lhasa block, the contact being marked by the Indus-Tsangpo suture zone (ITSZ). The amalgamation of the Tethyan Himalaya with the Lhasa block has been traditionally regarded as representing the India-Asia collision. Recently, however, a dual-collision model has been proposed, in which Tethyan Himalayais was considered as a separate block that rifted from Greater India’s northern margin in Late Cretaceous. The Tethyan Himalaya subsequently underwent two episodes of collision, i.e., the first with Lhasa block to the north ~50 Ma and the second collision with India to the south ~23 Ma. The dual-collision model hinges on the speculated rifting of Tethyan Himalaya from Greater India in Late Cretaceous, which, however, has not been paleomagnetically constrained because the Late Cretaceous paleomagnetic data from Tethyan Himalaya are lacking. Clearly, elucidating the Mesozoic, particularly the Late Cretaceous, tectonic evolution of Tethyan Himalaya is crucial to understanding the India-Asia collisional processes. To better constrain the paleogeographic position and drift history of Tethyan Himalaya during the Mesozoic, particularly in Late Cretaceous, a paleomagnetic investigation was conducted of the Xiare and Weimei (Jurassic) and Chuangde (Cretaceous) formations in the Chuangde areas of southern Tibet. Paleomagnetic samples were collected from 39 sites, among which 5 sites were from grey andesite of the Xiare Formation, 25 sites were from siltstone and sandstones of the Weimei Formation, and 9 sites were from limestones of the Chuangde Formation. A total of 118 paleomagnetic specimens were subjected to stepwise thermal or alternating field demagnetization. The demagnetization results show that samples from the Xiare Formation and the Weimei Formation did not yield characteristic remanent magnetization (ChRM). Specimens from the Chuangde Formation yield stable ChRMs upon demagnetization that display both normal and reversed polarities, and passed a reversal test. The anisotropy of magnetic susceptibility (AMS) data of samples from the Chuangde Formation show that the minimum axes are sub-vertical and the intermediate and maximum axes are subparallel to the bedding, indicative of a depositional-type fabric. Temperature-dependence magnetic susceptibility (*k-T* curves) and stepwise thermal demagnetization of the composite isothermal remanent magnetization (IRM) indicate that the remanence is carried principally by hematite and magnetite. Taken together, the sedimentological, rock magnetic, and paleomagnetic results suggest that the Chuangde ChRMs likely represent primary remanence that was acquired during 86.3–74.0 Ma, the age being constrained based on the foraminera data. The mean of the ChRMs of specimens from the Chuangde Formation is D_s=152.0°, I_s=–52.9°, κ=18.0, α_{95}=5.9° after tilt correction. The paleomagnetic results are interpreted to represent remanence of a normal polarity based on geological constraints and thus indicate that Tethyan Himalaya was located at 33.1°±5.6°S in Late Cretaceous (80.1±6.2 Ma). The paleolatitude of Tethyan Himalaya is similar to the coeval paleolatitude of India (reference site: 28.0°N, 88.5°E), suggesting that Tethyan Himalaya and India were not separated by oceans, but likely formed a single crustal block in the Campanian. It is possible that rifting took place afterwards. However, provenance studies of sediments in the middle Eocene (~45 Ma) Bhainskati Formation in Lower Himalaya have components sourced from the Tethyan Himalaya, suggesting that the Tethyan Himalya and India was then in immediate proximity. If the Tethyan Himalaya rifted from India after 74 Ma, it must have collided with India by ~45 Ma. This would require the development of and elimination of a ~1700-km-wide ocean within ~30 Myr, which is tectonically highly unlikely. Therefore, the paleomagnetic data obtained from the Chuangde Formation do not support the dual-collision model, but instead support the traditional model, that is the collision between Tethyan Himalaya and Lhasa block represents the India-Asia collision.

southern Tibet, Chuangde section, Tethyan Himalaya, Late Cretaceous, paleogeography, paleomagnetism

doi: 10.1360/N972016-00767